Local and nonlocal advection of a passive scalar

R. K. Scott
Northwest Research Associates, Bellevue, Washington 98009-3027

(Received 6 July 2006; accepted 23 August 2006; published online 7 November 2006)

Passive and active scalar mixing is examined in a simple one-parameter family of two-dimensional flows based on quasi-geostrophic dynamics, in which the active scalar, the quasi-geostrophic potential vorticity, is confined to a single horizontal surface (so-called surface quasi-geostrophic dynamics) and in which a passive scalar field is also advected by the (horizontal, two-dimensional) velocity field at a finite distance from the surface. At large distances from the surface the flow is determined by the largest horizontal scales, the flow is spectrally nonlocal, and a chaotic advection-type regime dominates. At small distances, z, scaling arguments suggest a transition wavenumber $k_c \sim 1/2z$, where the slope of the passive scalar spectrum changes from $k^{-5/3}$, determined by local dynamics, to k^{-1}, determined by nonlocal dynamics, analogous to the transition to a k^{-1} slope in the Batchelor regime in three-dimensional turbulence. Direct numerical simulations reproduce the qualitative aspects of this transition. Other characteristics of the simulated scalar fields, such as the relative dominance of coherent or filamentary structures, are also shown to depend strongly on the degree of locality. © *2006 American Institute of Physics*. [DOI: 10.1063/1.2375020]

I. INTRODUCTION

The large-scale, low-frequency motion of a rotating, stratified fluid is described to a good approximation by the quasi-geostrophic system, in which the dominant hydrostatic and geostrophic balances constrain particle trajectories to quasi-horizontal surfaces.[1] The system is completely described in terms of a single, materially advected quantity, the quasi-geostrophic potential vorticity $q(x,y,z,t)$, which is in turn related to the layerwise two-dimensional (2D) advecting flow through an inversion relation, $\psi = L(q)$, where L is some operator and $\psi(x,y,z,t)$ is the quasi-geostrophic streamfunction. In the simplest form, and scaling z according to the ratio of Coriolis and buoyancy frequencies, the equations take the form

$$q_t + J(\psi, q) = 0, \tag{1}$$

$$\Delta_3 \psi = q, \tag{2}$$

where $\Delta_3 = \partial_{xx} + \partial_{yy} + \partial_{zz}$ is the three-dimensional Laplacian operator and $J(f,g) = \partial_x f \partial_y g - \partial_x g \partial_y f$ is the two-dimensional Jacobian operator. In the case where the flow is semibounded in the vertical z, e.g., by a horizontal ground, an additional boundary condition is required, which typically takes the form of material advection of surface potential temperature, $\theta(x,y,t)$,

$$\theta_t + J(\psi, \theta) = 0, \tag{3}$$

$$\psi_z = \theta, \tag{4}$$

on the surface $z=0$.

Surface quasi-geostrophic (SQG) dynamics describes the particular situation when interior gradients of potential vorticity vanish and the flow is assumed to decay away from the single horizontal bounding surface, i.e., $q \equiv 0$ and $\psi \to 0$ as $z \to \infty$. In that case, the motion is determined entirely by the distribution of potential temperature on the single horizontal bounding surface. The system is then two-dimensional and the inversion relation between θ and ψ can be written as $-(-\Delta)^{1/2}\psi = \theta$, where Δ is the two-dimensional Laplacian.[2] The operator $(-\Delta)^{1/2}$ is defined most easily in spectral space,

$$\hat{\psi}(\mathbf{k}) = -|\mathbf{k}|^{-1}\hat{\theta}(\mathbf{k}), \tag{5}$$

which follows from (4) and (2) with $q \equiv 0$. Here $\hat{\psi}(\mathbf{k})$ is the Fourier transform of $\psi(x,y,t)$ and $\mathbf{k} = (k_x, k_y)$ is a two-dimensional horizontal wavenumber. Equation (5) can be compared with the case of the two-dimensional Euler equations (2DE), for which $\hat{\psi}(\mathbf{k}) = -|\mathbf{k}|^{-2}\hat{\omega}(\mathbf{k})$, where $\omega(x,y,t)$ is the vorticity, or the case of the full quasi-geostrophic equations (3DQG) with isothermal boundary conditions ($\theta|_{z=0} = 0$), for which $\hat{\psi}(\boldsymbol{\kappa}) = -|\kappa|^{-2}\hat{q}(\boldsymbol{\kappa})$, where $\boldsymbol{\kappa} = (k_x, k_y, k_z)$. In each case, the inversion results in a greater smoothing of the vorticity field than in SQG, which means that the flow at a given scale is controlled to a greater extent by larger scale structures. In this sense the dynamics of 2DE and 3DQG are nonlocal, whereas the dynamics of SQG is local.[3] Other basic properties of the SQG system, and how they differ from 2DE, have also been discussed in the literature.[2,4,5] Juckes[6] showed that the SQG system is equivalent to the quasi-geostrophic dynamics of the extratropical tropopause, which can be considered as a surface separating two regions of uniform potential vorticity across which the static stability is discontinuous.

Although the SQG system describes the evolution of a two-dimensional field it is derived in the context of a three-dimensional system in which the full streamfunction takes the form

$$\hat{\psi}(\mathbf{k}; z) = -|\mathbf{k}|^{-1}\hat{\theta}(\mathbf{k})e^{-|\mathbf{k}|z}. \tag{6}$$

Thus, structures in the flow decay away from the surface at a rate proportional their wavenumber. This gives rise to two

distinct regimes at a given distance, z_0: for $k=|\mathbf{k}| \ll 1/z_0$, the dynamics are essentially unchanged from SQG in that ψ satisfies (5), whereas for $k \gg 1/z_0$, $\hat{\psi}(\mathbf{k})$ is essentially zero. For large separations the dynamics is controlled entirely by the lowest wavenumbers.

In the present paper we examine the mixing of a passive scalar on surfaces for which $z \geqslant 0$. The special case of tracer mixing during vortex merger was considered recently by Wirth,[7] using a scalar field that was exactly correlated in z at $t=0$ (see discussion below). Here, on the other hand, we consider statistical properties of scalar mixing. For a given $z=z_0$, we again expect two distinct regimes: a local regime for $k \ll 1/z_0$, where scalar mixing at a given scale is dominated by the flow at that scale; and a nonlocal regime for $k \gg 1/z_0$, where scalar mixing is dominated by the flow at scales larger than z_0. For large z, the flow will have very little energy at small scales and a chaotic advection-type paradigm might be expected to hold, where all mixing is controlled by a spatially smooth, large-scale, and quasi-stationary flow.

This paper examines the transition between these two regimes and proposes this model as a useful framework in which to consider mixing in simply controlled local and nonlocal flows. In Sec. II, we review the relevant two-dimensional turbulence phenomenology and obtain predictions for scalar spectral shapes at general $z \geqslant 0$, the distance from the dynamical surface. In Sec. III, we present the results of direct numerical simulations (DNS) of the SQG system with passive scalar advection on $z \geqslant 0$ and examine in more detail the structure of the tracer field. In Sec. IV, we discuss implications for scalar mixing in various settings.

II. PHENOMENOLOGY

As for 2DE, the unforced SQG system possesses two invariants,[3]

$$\mathcal{E} = \frac{1}{A}\int_A \psi\theta dxdy \quad \text{and} \quad \mathcal{Z} = \frac{1}{A}\int_A \theta^2 dxdy, \tag{7}$$

with associated spectra $E(k)$ and $Z(k)$ defined by

$$\mathcal{E} = \int_0^\infty E(k)dk \quad \text{and} \quad \mathcal{Z} = \int_0^\infty Z(k)dk. \tag{8}$$

By analogy with 2DE, we may refer to $\mathcal{E}$ and $\mathcal{Z}$ as the energy and enstrophy, respectively. However, in SQG the quantity $\mathcal{Z}$ represents the surface potential energy and is equivalent to the velocity variance, or surface kinetic energy defined by $\mathcal{U}=1/A\int_A |\mathbf{u}|^2 dxdy$, where $\mathbf{u}=(-\psi_y,\psi_x)$ is the surface velocity. The quantity $\mathcal{E}$ represents the total, z-integrated, energy of the three-dimensional system, as originally noted by Blumen.[8] Hereafter, we refer to $\mathcal{E}$ as the total energy and $\mathcal{Z}\sim\mathcal{U}$ simply as the surface energy.

As is well known, the two invariants imply a dual cascade, in which surface energy is transferred to small scales (direct cascade) and total energy is transferred to large scales (inverse cascade). At equilibrium, the requirement that the surface energy flux ε to small scales be constant implies that the surface energy spectrum has the form[3,8] $Z(k)\sim U(k) \sim \varepsilon^{2/3}k^{-5/3}$, where $U(k)$ is the spectrum of $\mathcal{U}$ defined analogously to (8).

We consider next the properties of a passive scalar forced at large scales, and advected by the SQG flow according to

$$p_t + J(\psi,p) = 0. \tag{9}$$

Although all the dynamics take place on the surface, (9) is defined for $z \geqslant 0$ through (6) and we consequently examine scalar statistics for general $z \geqslant 0$. In general, the passive scalar spectrum $P(k)$ will satisfy

$$\chi(k) \sim kP(k)/\tau(k) \tag{10}$$

by dimensional arguments, where χ is the flux of scalar to small scales and $\tau(k)$ is a typical eddy turnover time at wavenumber k. On the surface itself, the dynamics are spectrally local so $\tau(k)$ can be written in terms of the surface energy, or velocity variance, at wavenumber k,

$$\tau(k) \sim [k^3U(k)]^{-1/2} \sim \varepsilon^{-1/3}k^{-2/3}. \tag{11}$$

The usual phenomenology[9,10] can then be applied under the assumption that the scalar flux $\chi(k)$ is constant at equilibrium. While the appearance of coherent structures in two-dimensional turbulence undermines the validity of this assumption, in practice, and as will be seen in the numerical results presented below, the constancy of the mean $\chi(k)$ is well satisfied here. Equations (10) and (11) then imply the scalar spectrum has the form

$$P(k) \sim \chi\varepsilon^{-1/3}k^{-5/3}. \tag{12}$$

For $z>0$, on the other hand, the dynamics cease to be local below a length scale defined by z, and the advective time scale at a given scale can no longer be written in terms of the energy at that scale. Instead, following the same procedure as for the weakly nonlocal case of the enstrophy cascade in two-dimensional flow,[11] we estimate the advective time scale at a given z, denoted by $\tau(k;z)$, in terms of the energy contained in all wavenumbers smaller than k,

$$\tau(k;z) = \left[\int^k k'^2 U(k';z)dk'\right]^{-1/2}, \tag{13}$$

where $U(k;z)$ is the spectrum of velocity variance at z. Using (6) it follows that

$$U(k;z) = Z(k)e^{-2kz}, \tag{14}$$

which makes explicit the exponential cutoff of kinetic energy at horizontal scales smaller than z. The asymptotic behavior of $\tau(k;z)$ is

$$\tau(k;z) \sim \begin{cases} \varepsilon^{-1/3}k^{-2/3} & \text{for } k \ll k_0, \\ \varepsilon^{-1/3}k_0^{-2/3} & \text{for } k \gg k_0, \end{cases} \tag{15}$$

for fixed $k_0=1/2z$. For $k \ll k_0$ the resulting $P(k)$ is as (12) for the surface case. For $k \gg k_0$, however, $P(k)$ is determined by the flow at the scale k_0, resulting in a Bachelor-type regime[12] with

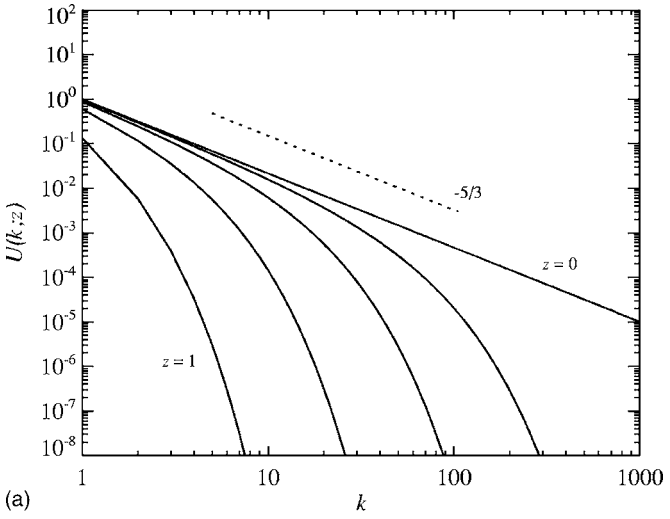

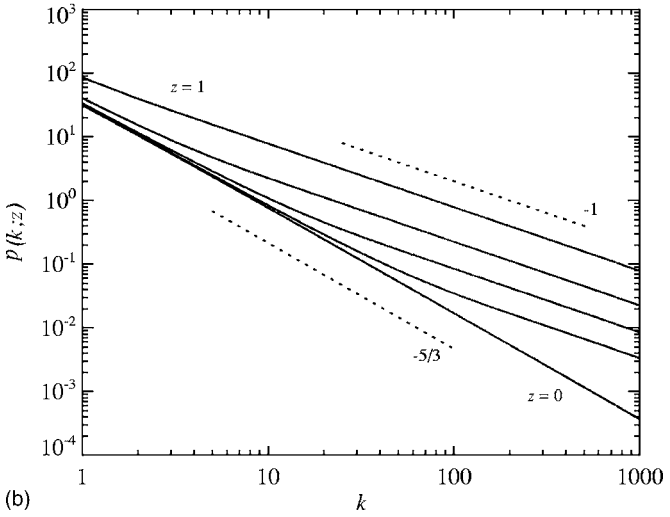

FIG. 1. Theoretical kinetic energy and passive scalar spectrum on and away from the surface, for $z=0,1/64,1/16,1/4,1$: (a) $U(k;z)$ as given by (14), with z increasing downward from the surface $k^{-5/3}$ slope. (b) $P(k;z)$ as given by (10) and (13) with a low wavenumber cutoff at $k_f=1$ and z increasing upward.

$$P(k;z) \sim \chi\varepsilon^{-1/3}k_0^{-2/3}k^{-1}. \tag{16}$$

Figure 1 shows the kinetic-energy spectrum, $U(k;z)$, as given by (14), and the passive scalar spectrum $P(k;z)$ based on (13), for $z=0,1/64,1/16,1/4,1$, with an energy injection scale at $k_f=1$. The special case $z=0$ corresponds to flow and scalar advection on the surface, in which case $P(k)$ follows the pure $k^{-5/3}$ spectrum given by (12). As z increases, the energy at high wavenumbers is more and more strongly attenuated, until at $z=1$ only the lowest wavenumbers contain significant energy. The corresponding $P(k)$ approaches a k^{-1} spectrum at all wavenumbers. For intermediate z, $P(k) \sim k^{-5/3}$ for wavenumbers $k<k_0=1/2z$, and transitions to a k^{-1} spectrum for $k>k_0$.

III. DIRECT NUMERICAL SIMULATION

We now test the theoretical spectral shapes with direct numerical simulations of the forced-dissipative equations

$$\theta_t + J(\psi,\theta) = \nu_l\Delta^l\theta + \nu_h\Delta^h\theta + F^{(\theta)}, \quad z=0, \tag{17a}$$

$$p_t + J(\psi,p) = \nu_l\Delta^l p + \nu_h\Delta^h p + F^{(p)}, \quad z>0, \tag{17b}$$

with $\psi=\psi(x,y,z,t)$ related to $\theta(x,y,t)$ through (6). We consider p defined on discrete levels $z=0,1/64,1/16,1/4,1$.

Both the active scalar and the passive scalar are forced at large scales. The spectrum of the forcing functions $F^{(\theta,p)}$ is given by

$$\hat{F}(k) = \begin{cases} \eta/\Delta k & |k-k_f| \leqslant \Delta k/2, \\ 0 & \text{otherwise}, \end{cases} \tag{18}$$

where $k_f=5$, $\Delta k=1/\sqrt{2}$, and where $\eta=1$ is the constant input rate of surface energy and scalar variance. The time dependence of the forcing is Markovian and for each spectral mode with $\mathbf{k}$ satisfying $|k-k_f|\leqslant\Delta k/2$ is determined by

$$\hat{F}(\mathbf{k},t+\delta t) = (1-r^2)^{1/2}e^{i\varphi} + r\hat{F}(\mathbf{k},t), \tag{19}$$

where φ is a random phase, and where r is defined through the decorrelation time $c_r=\delta t/(1-r)=0.1$. At each time step (19) is normalized so that the injection rate of surface energy and scalar variance is constant and equal to $\eta=1$. The forcing of each field is independent so the passive scalar evolution on each z is uncorrelated, and uncorrelated from the active scalar.

Energy is removed at large scales by the hypodiffusion term $\nu_l\Delta^{-l}$ in (17), with $l=-2$ and $\nu_l=0.01$, i.e., a damping time scale of $\tau_l=100$ at the largest $(k=1)$ spatial scales. These values have been chosen to allow equilibration of the larger scale fields, while having minimal influence on the inertial range $k>k_f$. At small scales, a high-order hyperdiffusion with $h=4$ is used ensure numerical stability while allowing a large inertial range at modest resolution. The diffusion coefficients are determined by the rms velocity field on each level, which defines a straining time scale at the smallest spatial scales, $\tau_h=u_{\text{rms}}k_{\max}$, where $k_{\max}$ is the maximum resolved wavenumber.[13] This ensures comparable diffusion rates for both θ and p across the different levels. Specifically, we have $\nu_h k_{\max}^{2h}=2,1.85,1.57,0.96,0.20$ on $z=0,1/64,1/16,1/4,1$, estimated from preliminary simulations. Again, these values of h and ν_h ensure that dissipation is essentially zero in the inertial range under consideration.

From (11), the time scale of the flow tends to zero at large k, which means a short time step is required for numerical stability. On the other hand, for $z>0$ the flow is weak and a long integration time is required to reach equilibrium. Since lower wavenumbers decay more slowly in z and so contribute the most energy to the flow at $z>0$, the situation is ameliorated if large-scale structures can develop freely in the inverse cascade. For this reason, a second set of simulations was performed without hypodiffusion or other large-scale dissipation. In this case, equilibrium is never completely reached but the effect on the high wavenumber spectral shapes over the time periods considered was small.

We use a fully dealiased pseudospectral method to solve (17) on a doubly periodic horizontal domain $(x,y) \in [-\pi,\pi]\times[-\pi,\pi]$, with ψ and p defined on the surfaces $z\geqslant 0$ defined above, starting from zero initial conditions. The

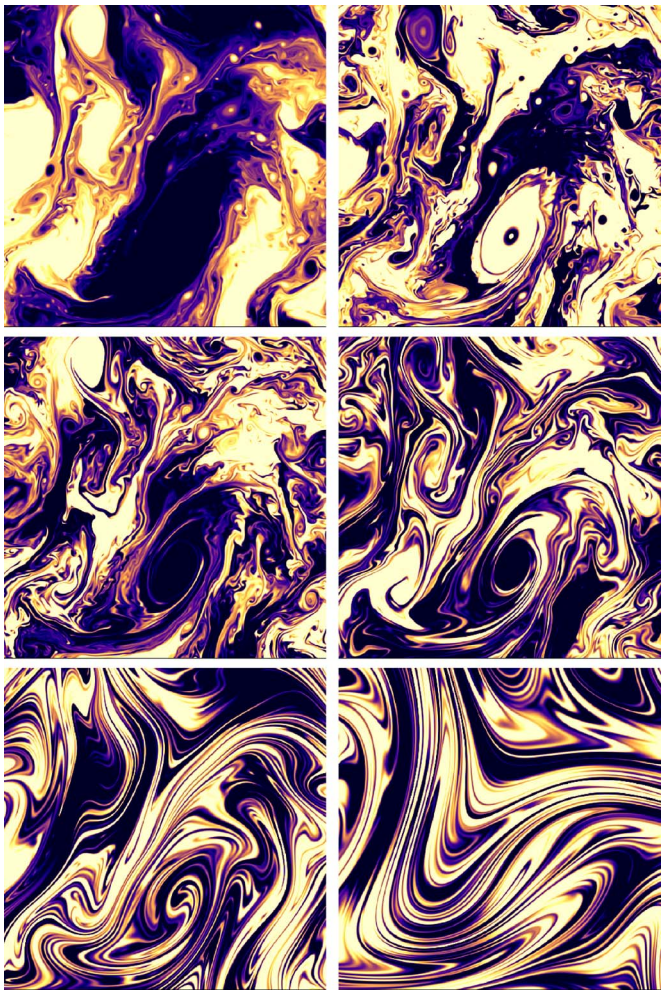

FIG. 2. (Color online) Simultaneous snapshot of surface θ (top left) and passive scalar p on $z=0$, $z=1/64$, $z=1/16$, $z=1/4$, and $z=1$ (left to right, top to bottom). The color scale in each panel has been normalized according to the rms value of each field: darkest and lightest represent extreme positive and negative values. One-sixteenth of the computational domain is shown with $-\pi/4 \leqslant x,y \leqslant \pi/4$; the forcing scale is $k_f^{-1}=1/5$.

time stepping is a fourth-order Runga-Kutta scheme, with the forcing and diffusion terms treated implicitly. We increase the resolution incrementally from 256×256 grid points to 2048×2048. The spectral shapes at high wavenumbers are allowed to equilibriate at each resolution. At the highest resolution, the equations are integrated for approximately 40 turnaround times of the largest-scale (and slowest) eddies.

Figure 2 shows a simultaneous snapshot of the surface potential temperature θ and passive scalar fields p at $z=0,1/64,1/16,1/4,1$. Before discussing the spectral behavior, we make a few qualitative observations based on the two-dimensional scalar fields. A number of features are worth noting.

(i) In the θ field, the presence of long-lived coherent structures is clear. Although their presence impairs the convergence of higher-order statistics, reasonable convergence of spectra in the surface energy cascading regime was nevertheless achieved in all the simulations considered (with or without large-scale dissipation).

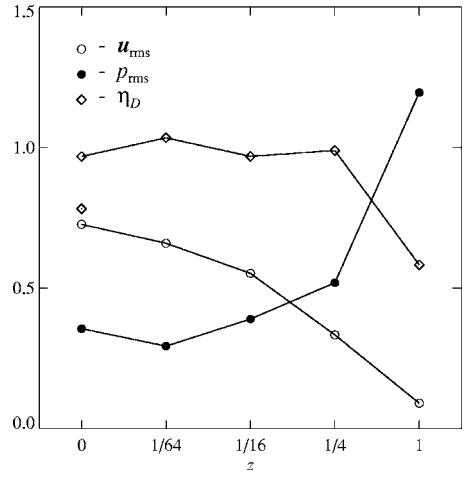

FIG. 3. Rms velocity, $\mathbf{u}_{\rm rms}$, passive scalar $p_{\rm rms}$, and scalar dissipation η_D (scaled to fit axes) as a function of z. Note that $\theta_{\rm rms}=\mathbf{u}_{\rm rms}(z=0)$. The solitary diamond denotes the dissipation for the active scalar on $z=0$. Arbitrary units.

(ii) The active and passive scalar fields on the surface $z=0$ share a broadly similar structure, although p appears more filamentary than θ. The greater filamentary structure of p is verified by the power spectra and two-point probability density functions described below. The differences in structure are consistent with higher-resolution simulations performed recently by Celani *et al.*,[14] who found rougher p in simulations with forcing that was delta correlated in time.

(iii) In the passive scalar field, there is a systematic increase in the proportion of filamentary to coherent structures with increasing z. For the lower two cases, $z=1/4$ and $z=1$, the scalar field is dominated by filamentary structures. For $z=1$ the scalar structure resembles that of chaotic advection flows, arising from repeated stretching and folding by the large-scale flow.

(iv) The passive scalar field on $z=0$ exhibits intense coherent structures at all scales, as for the active field. On $z>0$, on the other hand, p only exhibits coherent structures at scales larger than a given scale, which varies directly with z. In other words, there is a systematic elimination of coherent structures at progressively larger scales as z increases, due to the exponential cutoff of energy at wavenumbers beyond $k_0=1/z$. Coherent scalar structures result from the trapping of scalar values in coherent flow structures, which decay exponentially in z at a rate proportional to their wavenumber.

(v) Mixing efficiency of p, as defined by the generation of small-scale filamentary structures, increases with z; in particular, at small z, coherent structures inhibit mixing by trapping of extreme scalar concentrations. However, because the energy of the flow decreases with z, the actual mixing rate is not necessarily monotonic in z. This is illustrated in Fig. 3. The rms velocity $\mathbf{u}_{\rm rms}$ (open circles) decreases sharply with z because of the attenuation of the small-scale flow. The

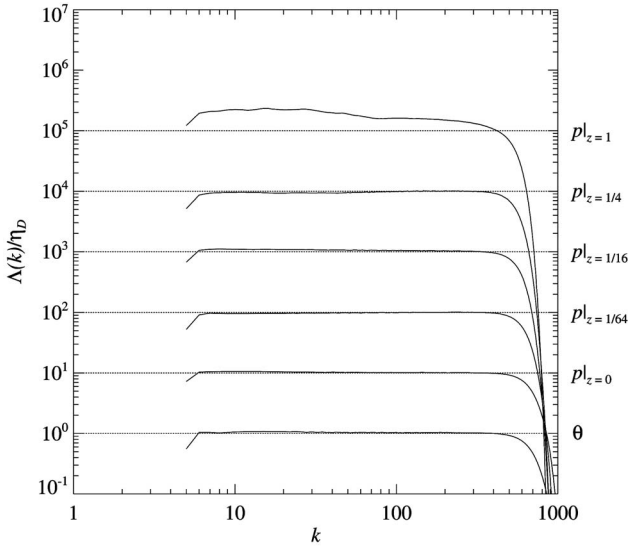

FIG. 4. Spectral flux of surface energy and passive scalar variance $\Lambda(k)$ divided by η_D. Lines are shifted for clarity; labels on right-hand axes are located at unity each field.

scalar dissipation is also shown (diamonds), which shows that the mixing rate is approximately uniform in z: at large z, the more filamentary scalar field is compensated by the less energetic flow. (Note that the scalar dissipation on $z=1$ is not fully equilibriated but is still growing in time.) Finally, the approximately uniform mixing rates are reflected in the rms scalar value p_{rms}, which can again be interpreted as a crude measure of mixing rate (since scalar input is constant).

Because the flow is very weak on $z=1$ a longer time is needed to reach stationarity than for smaller z. The scalar dissipation reaches a constant value in all other cases, but is still increasing on $z=1$ by the end of the simulation (not shown). The spectral flux, plotted in Fig. 4, shows that an equilibrium between scalar flux and dissipation is not achieved on $z=1$. For smaller z, equilibrium is generally reached over a large inertial range, although in some cases there is a deficit of scalar transfer at low wavenumbers. Unlike in 2DE, the eddy turnaround time in the present case varies indirectly with wavenumber, resulting in a more rapid equilibration at small scales than at large scales. Hence, although the scalar dissipation equilibriates quickly, it takes longer for a stationary inertial range to develop at large scales. In Fig. 4 and hereafter all quantities are averaged in time over the last half of the simulation, long after scalar dissipation has equilibriated for all cases $z<1$.

Figure 5 shows the computed kinetic energy and scalar spectra for the same values of z. The surface kinetic-energy spectrum $U(k;0)$ [equivalently, the active scalar variance $Z(k)$] has a slope of around -1.7 broadly consistent with the predicted spectrum. This computed slope is consistent with that found in the recent high-resolution simulations reported by Celani *et al.*[14] (1.80 ± 0.1). Both slopes are closer to the predicted spectrum than earlier studies either at lower resolution[3] or using ordinary diffusion,[15] supporting Schorghofer's conclusion[15] that increasing Reynolds number leads to flatter spectral slopes in the SQG direct cascade. On surfaces for which $z>0$, the kinetic-energy spectrum $U(k;z)$ is modified according to (14) and each curve is simply reduced by a factor e^{-2kz}. This strongly attenuates the kinetic energy at large k. The effect of the attenuation is also visible in the reduction in the spectral peak at $k=2$.

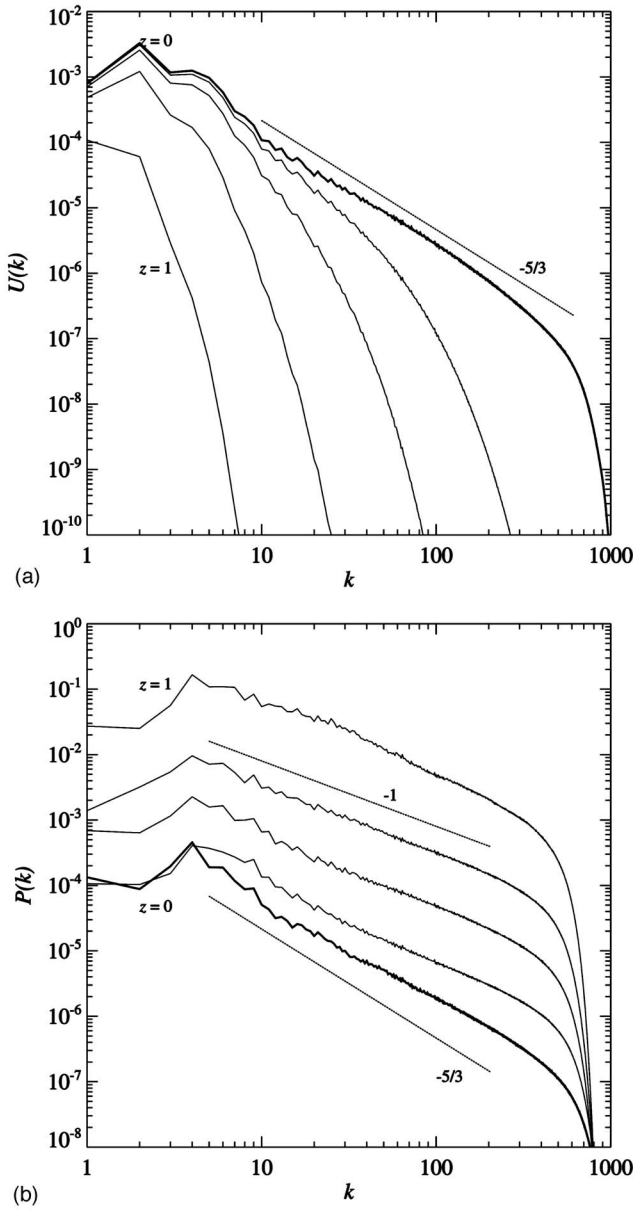

FIG. 5. Kinetic energy and passive scalar spectrum from DNS on and away from the surface, for $z=0,1/64,1/16,1/4,1$: (a) $U(k;z)$ with z increasing downward. (b) $P(k;z)$ with z increasing upward. Bold lines denote values on $z=0$. In (b) consecutive lines are shifted half a decade vertically for clarity. Note that in (a), $Z(k)\equiv U(k;0)$.

The passive scalar spectrum on $z=0$ is flatter than predicted, with a slope of -1.4 ± 0.06, consistent with the rougher scalar field seen in Fig. 2. As in Celani *et al.*,[14] we therefore find a difference in the behavior of the active and passive scalar fields on $z=0$ already in the low-order statistics, and a departure from the theoretical prediction (12). Note also that the passive scalar spectrum is shallower than

would be expected using (11) with the computed spectral slope of −1.7 for $U(k)$.

For $z>0$, there is a further flattening of the passive scalar spectra, qualitatively similar to that described in Sec. II. First, for $z=1/64$, the spectrum flattens to a slope slightly greater than −1 at wavenumbers higher than about $k=30$, while for $k<30$ the slope is closer to the predicted −5/3. The structure is roughly consistent with the predicted structure (cf. Fig. 1). For $z=1/16$, the flattening occurs at lower wavenumbers, near $k=10$, and it becomes difficult to identify a local inertial range between here and the forcing wavenumber $k_f=5$. For $z=1/4$ and $z=1$, no local range is present and the spectrum has a roughly −1 slope everywhere, determined by the energy in the lowest wavenumbers. Again, note that for $z=1$ the spectrum takes longer to reach convergence because the flow is less energetic, and has not yet equilibriated at small scales. The cleanest −1 slope is obtained at $z=1/4$ across over a decade of wavenumbers.

The probability density function (pdf) of scalar increment, $\delta_r\theta$ and $\delta_r p$, where $\delta_r\phi=\langle\phi(\mathbf{x}-\mathbf{r})-\phi(\mathbf{r})\rangle$, provides a useful way to quantify the change in scalar structure with increasing z. Figure 6 shows the pdf of scalar increment normalized by the standard deviation σ, for values of r from 0.0125 to 0.2. On $z=0$ the active scalar displays a strong level of intermittency, but with considerable variation with r: the tails of $\delta_r\theta$ are flatter than exponential at small r but become steeper than exponential, though not quite Gaussian, at large r. The flatness structure function $S_4(r)/[S_2(r)]^2$ (not shown) varies from around 4 at large r to over 10 at small r. For the passive scalar, on the other hand, $\delta_r p|_{z=0}$ has clearly broader than exponential tails over the full range of r, with $S_4(r)/[S_2(r)]^2$ taking values approximately between 8 (large r) and 20 (small r).

As z increases from 0 there is a qualitative change in the character of the pdfs of the passive scalar. For $z=1/64$, the dependence on r is similar to that found for the active scalar. Again, anomalous scaling (i.e., departure from Gaussian shape) appears across the full range of r values but is strongest at small r. As z increases further, anomalous scaling diminishes overall but persists to some extent at small r. For $z=1/4$ and $z=1$ the large r behavior approaches normal scaling with approximately Gaussian tails and $S_4(r)/[S_2(r)]^2 \sim 3$. The broad, irregular tails at small r in the case $z=1$ are most likely due to the slowness of convergence of the small scales, described above, although it appears that anomalous scaling persists.

IV. DISCUSSION

We have introduced a one-parameter family of flows based on the surface quasi-geostrophic system, whose effect on passive scalar mixing ranges from local to nonlocal. In effect, the system comprises a flow that is filtered at progressively larger scales. Equivalently, the parameter z can be thought of as controlling the scale below which the flow is rough. Scaling arguments suggest a passive scalar spectrum that shallows to k^{-1} at wavenumbers larger than $1/2z$. Passive scalar spectra obtained from direct numerical simulations are in qualitative agreement with the predicted spectra.

For the special case of $z=0$ corresponding to the surface quasi-geostrophic system, the spectral shape of the active scalar is broadly consistent with theoretical expectations. On the other hand, the passive scalar is considerably rougher and has a shallower spectrum than that predicted on the basis of the energy spectrum. These results are consistent with recent high-resolution simulations of surface dynamics[14] that also found shallower spectra for the passive scalar than active scalar. Differences between the scaling properties of the active and passive scalar are also apparent from consideration of the pdfs of scalar increment.

Spectral scaling properties of local and nonlocal dynamics have been previously considered in the context of a simple one-parameter family of models ranging from spectrally nonlocal for $\alpha>2$ to local for $\alpha<2$, where $\alpha/2$ is the exponent of the Laplacian relating streamfunction and vorticity.[3] The marginal case ($\alpha=2$) in that family corresponds to the 2D barotropic equations, whose kinetic energy scales as k^{-3} in the enstrophy cascading range. SQG corresponds to the case $\alpha=1$. The family of models described in the current paper is proposed as an alternative bridge between local and nonlocal dynamics, where here the scales at which nonlocal effects become important are controlled directly through z. The range of passive scalar structure obtained with varying z, dominated by coherent structures on all scales at one extreme, and by pure filamentary structures at the other extreme, is immediately obvious in Fig. 2.

Beyond its use as an intermediate model bridging local and nonlocal dynamics, the present model has direct applications in various geophysical situations, wherever the dynamics evolves according to a surface potential temperature distribution, either at a solid surface or at an internal interface separating two regions of different static stability. An example of the latter occurs at the extratropical tropopause.[6] The dynamics in this region can be contrasted with that of the winter stratosphere, where the velocity field is dominated by coherent, large-scale structures, and where the chaotic advection paradigm, an extreme example of nonlocal dynamics, is a good approximation.[16,17] As a consequence, a good representation of stratospheric mixing properties of the flow can be obtained with relatively coarse resolution wind fields.[18] In the troposphere and lower stratosphere, on the other hand, the kinetic-energy spectrum is shallower and the dynamics are more local. At the tropopause itself, the jump in static stability implies a potentially stronger role for surface dynamics.[6] Close to the tropopause the structure of chemical tracer mixing might be expected to contain features anticipated by the present work. Mixing properties near the tropopause play an important role in the general circulation of the whole atmosphere and so the question of whether the dynamics near the tropopause is dominated by nonlocal or local behavior is clearly of interest.

Finally, it is interesting to relate the present results to the recent study by Wirth *et al.*,[7] which also considered aspects of mixing on horizontal surfaces at $z>0$ in the SQG framework. Rather than the transition from local to nonlocal mixing, that study focused on the transition from active to passive scalar mixing, by considering a passive scalar that was exactly correlated with the active scalar θ on the surface

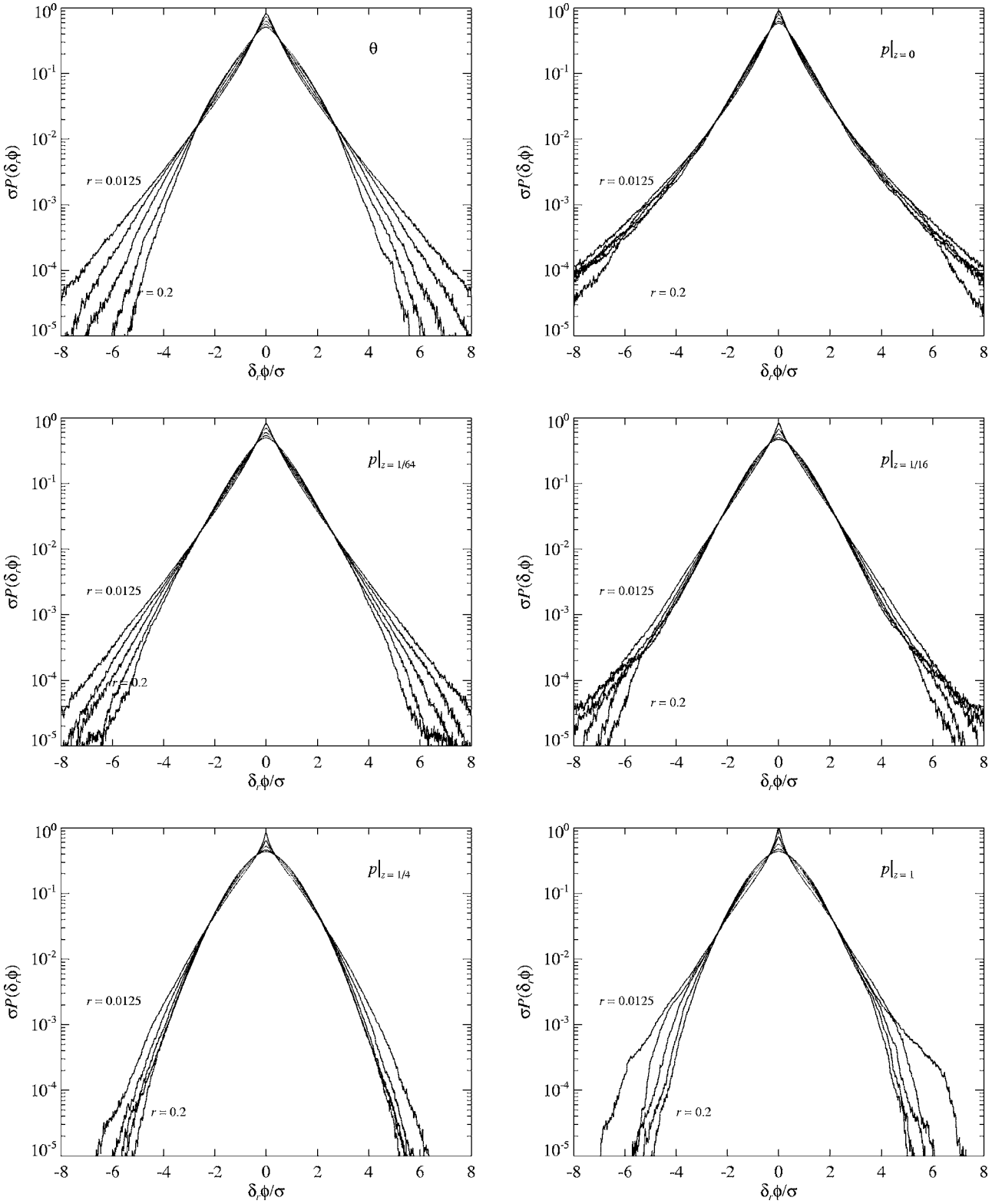

FIG. 6. Probability distribution function of scalar increment for separations $r=0.0125, 0.025, 0.05, 0.1, 0.2$, normalized by standard deviation. Left to right and top to bottom: active scalar $\delta_r\theta$, passive scalar $\delta_r p$ on $z=0, 1/64, 1/16, 1/4, 1$.

$z=0$, and which became progressively decorrelated for increasing $z>0$. One central result of that study was that mixing (as defined by contour lengths) maximizes for small but finite $z>0$. This was interpreted as a consequence of two compensating factors: the decrease in flow intensity and the decrease in correlation between passive and active scalar with increasing z. The present results differ in that the correlation between passive and active scalar is exactly zero for all z, but similar arguments apply. Figure 2 suggests that the most efficient mixing is achieved for $z=1$, when mixing efficiency is defined as scalar dissipation for a given flow energy: only on $z=1$ is there a complete absence of scalar

trapping in coherent structures. On the other hand, the energy of the flow on $z=1$ is very weak and the time scale required to achieve a completely mixed state is long. Thus the mixing rate, as measured by the scalar dissipation, is nonmonotonic in z, and in fact appears to be nearly independent of z at small $z>0$. More accurate quantification of the mixing rate is currently under investigation.

ACKNOWLEDGMENTS

The author wishes to thank Peter Haynes and Volkmar Wirth for interesting and informative discussions during the preparation of this work. Financial support was provided by the National Science Foundation.

[1] J. Pedlosky, *Geophysical Fluid Dynamics* (Springer, Berlin, 1987).
[2] P. Constantin, A. J. Majda, and E. Tabak, "Singular front formation in a model for quasigeostrophic flow," Phys. Fluids **6**, 9 (1994).
[3] R. T. Pierrehumbert, I. M. Held, and K. L. Swanson, "Spectra of local and nonlocal two-dimensional turbulence," Chaos, Solitons Fractals **4**, 1111 (1994).
[4] I. M. Held, R. T. Pierrehumbert, S. T. Garner, and K. L. Swanson, "Surface quasi-geostrophic dynamics," J. Fluid Mech. **282**, 1 (1995).
[5] J. Sukhatme and R. T. Pierrehumbert, "Surface quasigeostrophic turbulence: The study of an active scalar," Chaos **12**, 439 (2002).
[6] M. N. Juckes, "Quasigeostrophic dynamics of the tropopause," J. Atmos. Sci. **51**, 2756 (1994).
[7] V. Wirth, H. Borth, J.-F. Lopez, W.-G. Panhans, M. Riemer, and T. Szabo, "Dynamics of extratropical tropopause region: a case of transition between dynamically active and passice tracer advection," Q. J. R. Meteorol. Soc. **131**, 247 (2005).
[8] W. Blumen, "Uniform potential vorticity flow. Part I: Theory of wave interactions and two-dimensional turbulence," J. Atmos. Sci. **35**, 774 (1978).
[9] A. M. Obukhov, "The structure of the temperature field in a turbulent flow," Izv. Akad. Nauk SSSR, Ser. Geogr. Geofiz. **13**, 58 (1949).
[10] S. Corrsin, "On the spectrum of isotropic temperature fluctuations in isotropic turbulence," J. Appl. Phys. **22**, 469 (1951).
[11] R. H. Kraichnan, "Inertial ranges in two-dimensional turbulence," Phys. Fluids **10**, 1417 (1967).
[12] G. K. Batchelor, I. D. Howells, and A. A. Townsend, "Small-scale variation of convected quantities like temperature in turbulent fluid. Part II: The case of large conductivity," J. Fluid Mech. **5**, 134 (1959).
[13] M. E. Maltrud and G. K. Vallis, "Energy spectra and coherent structures in forced two-dimensional and beta-plane turbulence," J. Fluid Mech. **228**, 321 (1991).
[14] A. Celani, M. Cencini, A. Mazzino, and M. Vergassola, "Active and passive fields face to face," New J. Phys. **6**, 72 (2004).
[15] N. Schorghofer, "Energy spectra of steady two-dimensional turbulent flows," Phys. Rev. E **61**, 6572 (2000).
[16] K. Ngan and T. G. Shepherd, "A closer look at chaotic advection in the stratosphere. Part I: Geometric structure," J. Atmos. Sci. **56**, 4134 (1999).
[17] K. Ngan and T. G. Shepherd, "A closer look at chaotic advection in the stratosphere. Part II: Statistical diagnostics," J. Atmos. Sci. **56**, 4153 (1999).
[18] P. Bartello, "Using low-resolution winds to deduce fine structure in tracers," Atmos.-Ocean. **38**, 303 (2000).